metals

MDPI

Article

Effect of Sample-Size on the Compression Deformation Behavior of a CuZr-Based Bulk Metallic Glass Composite

Yongsheng Chen [1], Weizhong Liang [1,*], Longxing Wang [1], Kai Qi [1], Yang Wang [1], Xiaomei Sun [2] and Naiwen Fang [2]

[1] School of Materials Science and Engineering, Heilongjiang University of Science and Technology, Harbin 150022, China; chenyongsheng111@126.com (Y.C.); wanglongxing199408@126.com (L.W.); qikai19950101@126.com (K.Q.); wangyang199608@163.com (Y.W.)

[2] Harbin Welding Institute Limited Company, Harbin 150028, China; sunxiaomei_2011@163.com (X.S.); naiwen20@163.com (N.F.)

* Correspondence: wzliang1966@126.com; Tel./Fax: +86-451-88036219

Received: 4 May 2020; Accepted: 27 June 2020; Published: 28 June 2020

Abstract: The compressive deformation behaviors and microstructures of $Cu_{45}Zr_{48}Al_4Nb_3$ bulk metallic glass composites with diameters of 3, 2, and 1 mm were investigated systematically. It was found that the smallest sample showed the highest yield strength and compressive plasticity. The yield strength of the samples was found to depend on the fraction of their crystalline phases in the glassy matrix. The smaller samples showed larger free volumes, which is favorable for plastic deformation. The deformation behavior of the samples was found to depend on their size. The results obtained in this study will be helpful for investigating the mechanical behavior of metallic glass composites.

Keywords: bulk metallic glass composite; sample-size; deformation behavior; plasticity

1. Introduction

Due to their high strength, low elastic modulus, and good wear resistance, bulk metallic glasses (BMGs) have gained significant attention for practical applications. However, the inadequate plastic deformation of BMGs at room temperature limits their practical applications [1–4]. In recent years, various efforts have been made to overcome this limitation. It has been reported that the formation of BMG composites (BMGCs) is an effective approach to improve the room-temperature plasticity of BMGs [5–7]. CuZr-based BMGs exhibit excellent glass-forming ability. The addition of Ta and Nb to BMGs can result in the formation of BMGCs [8–13]. Such BMGCs show optimum plasticity at room temperature, as evidenced by their typical stress–strain curves with serration flows [14–17]. It has been reported that the microstructure and mechanical properties of BMGs depend significantly on their sample-sizes. Wu et al. [18] investigated the effect of the sample-size on the failure mode and compressive plasticity of different BMGs. They found that the plasticity of the samples was significantly affected by their cooling rate and sample-size. Xiao et al. [19] reported that a decrease in the sample-size of TiZrCuNi BMGs increased their cooling rate and compressive plasticity. However, the effect of the cooling rate on the compressive properties of BMGCs is still unclear. Hence, the cooling rate of BMGCs should be adjusted in order to further improve their compressive plasticity. In this study, we successfully fabricated $Cu_{45}Zr_{48}Al_4Nb_3$ BMGC samples with diameters of 3, 2, and 1 mm and investigated the effect of sample-size on their microstructures and compressive deformation behaviors.

2. Experimental Procedure

The $Cu_{45}Zr_{48}Al_4Nb_3$ BMGCs were fabricated by electric arc melting the raw materials (purity > 99.9%) in a Ti-gettered argon atmosphere. The ingots were re-melted five times in order to ensure compositional homogeneity. Cylindrical samples with a length of 50 mm and different diameters of 1, 2, and 3 mm were prepared using a copper mold via the suction-casting method. The phase structures of the test specimens were examined by x-ray diffraction (XRD) with Cu-Kα radiation (λ = 1.5405 Å, 2θ = 20°–80°, step size of 0.02°). The XRD specimens were cut from the cylindrical sample by wire cutting and then the cross-section was ground with abrasive paper. The thermal analysis of the test specimens was carried out using differential scanning calorimetry (DSC, Netzsch STA449-F3) at a heating rate of 0.33 K/s. The microstructures of the cast samples were analyzed using an optical microscope (OM, Carl Zeiss, Shanghai, China) and transmission electron microscopy (TEM, JEM-2010F). The TEM samples were prepared by mechanically grinding and electrolytic double spraying in a mixed solution of perchloric acid and methanol (the current of double spraying was 4.5 A). Compression samples with the diameters of 1, 2, and 3 mm and heights of 2, 4, and 6 mm were prepared. Quasi-static compression tests were carried out on a testing machine (Product model INSTRON-5569, Canton, OH, USA,) at room temperature at a constant strain rate of 3×10^{-4} s^{-1}. Each compression experiment was repeated six times. The surfaces of the fractured specimens were examined by scanning electronic microscopy (SEM, MX2600FE, Leoben, Austria).

3. Results and Discussion

Figure 1 shows the XRD patterns of the $Cu_{45}Zr_{48}Al_4Nb_3$ BMGC samples with the diameters of 1, 2, and 3 mm. The XRD patterns of the samples exhibited only one broad diffraction peak, indicating that the samples showed a glassy structure. The higher diffraction peak intensity means a larger number of glassy structure. Compared with the 2 mm and 1 mm samples, a small diffraction peak intensity was observed on the 3 mm sample, which means that the 3 mm sample may have some crystalline particles.

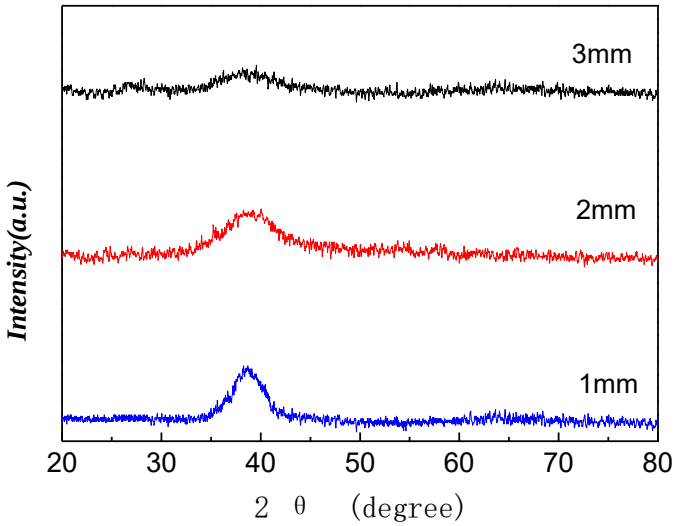

Figure 1. X-ray diffraction (XRD) patterns of the $Cu_{45}Zr_{48}Al_4Nb_3$ BMGC samples with the diameters of 3 mm, 2 mm, and 1 mm.

The DSC curves of the BMGC samples with the diameters of 1, 2, and 3 mm are shown in Figure 2. Figure 2a shows that the glass transition of the samples was followed by an exothermic crystallization heat event. The 3 mm sample exhibited the smallest heat release region among all the samples. This indicates that the 3 mm sample exhibited the largest crystalline phase fraction among all the samples. As can be observed from Figure 2b, the enthalpy release (ΔH) values of the 1, 2, and 3 mm samples were 2.3, 1.6, and 1.1 J/g, respectively. The enthalpy release of the samples was

linearly proportional to their free volume contents [20]. This indicates that the 1 mm sample showed the largest free volume. The previous study reported that the enthalpy release of the samples can reflect the content of crystalline phase in the specimen. The smaller the enthalpy release, the higher the content crystalline phase in the specimens [20]. Therefore, compared with the 1 mm sample, the 3 mm sample contained some crystalline particles. The cooling rates of the samples were calculated using the following equation: T (K/s) = $10/R^2$ (cm) [21], where T is the achieved cooling rate and R is the radius of the as-cast samples. The cooling rates of the 1, 2, and 3 mm samples were calculated to be 4000, 1000, and 444 K/s, respectively. Hence, the cooling rates of the samples depended on their as-cast diameters. An increase in the cooling rate can increase the free volume of BMGCs [22]. Hence, the 1 mm sample exhibited higher free volume than the other two samples.

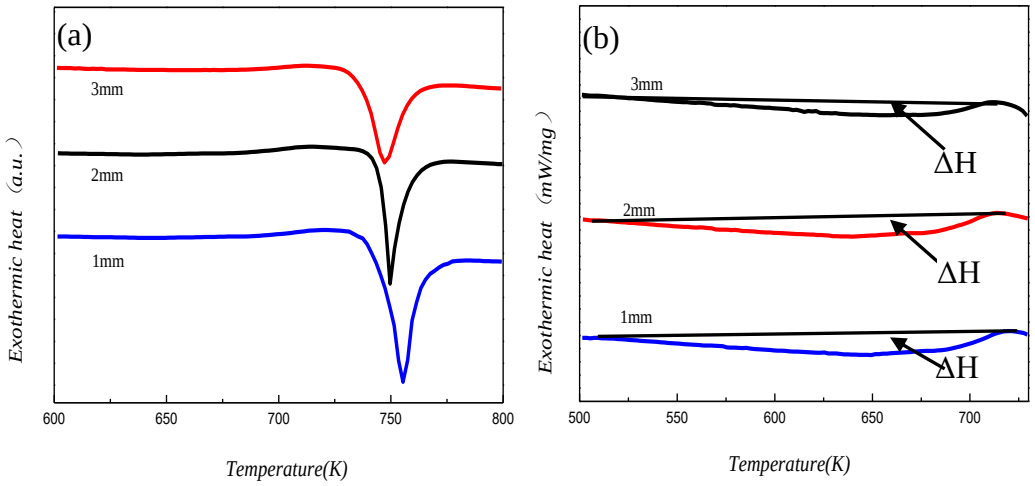

Figure 2. Differential scanning calorimetry (DSC) curves of the $Cu_{45}Zr_{48}Al_4Nb_3$ BMGC samples with different diameters, (**a**) in the temperature range of 600–800 K, (**b**) is the magnified view of (**a**).

Figure 3 shows the OM images of the cross-sectional microstructures of the $Cu_{45}Zr_{48}Al_4Nb_3$ BMGC samples with different diameters. The 1 mm sample exhibited an almost glassy microstructure with few crystalline phases. The 2 and 3 mm samples exhibited a few spherical grains with different sizes. This indicates that the samples showed different microstructures during the rapid solidification process. The content of crystalline phase was roughly estimated by DSC. However, in order to precisely describe this, further experiments are needed to confirm this [23,24].

Figure 4 shows the compressive strain–stress curves of the three $Cu_{45}Zr_{48}Al_4Nb_3$ BMGC samples with different diameters. The three samples exhibited considerable plastic deformation during the quasi-static compression process (Figure 4a). The 1 mm sample exhibited higher yield strength and plastic strain (1720 ± 60 MPa and 6.7%) than the 2 mm (1625 ± 60 MPa and 1.2%) and 3 mm (1610 ± 60 MPa and 0.8%) samples. In contrast, the 1 mm sample also exhibited lower value of elastic modulus (88.0 ± 0.5 GPa) than the 2 mm (93.2 ± 0.4 GPa) and 3 mm (93.7 ± 0.5 GPa) samples. The modulus of the amorphous phase was lower compared with the crystalline one [2,3]. The results suggest that the 3 mm sample had the largest number of crystalline fraction, which is consistent with the DSC results obtained in this study. Hence, the smallest sample showed the highest yield strength and plasticity with serrated flow. The serrated flow behavior of the sample can be attributed to the formation of shear bands. The serrated flow of the samples increased with a decrease in their diameter (Figure 4b). The serration event included the accumulation of elastic energy and the consumption of elastic energy, which led to the production of the shear band [25]. As shown in the inset of Figure 4b, larger stress-drop implied higher elastic energy released, resulting in more shear bands. The 1 mm sample showed the largest serrated flow among all the samples, indicating that it formed the largest number of shear bands among all the samples before compression fracture. Zhang et al. reported that the serrated flow behavior of BMGCs significantly depended on their free volume [26]. This is

consistent with the DSC and OM results obtained in this study. The results suggest that the yield strength and plastic deformation of the samples were affected by their diameter.

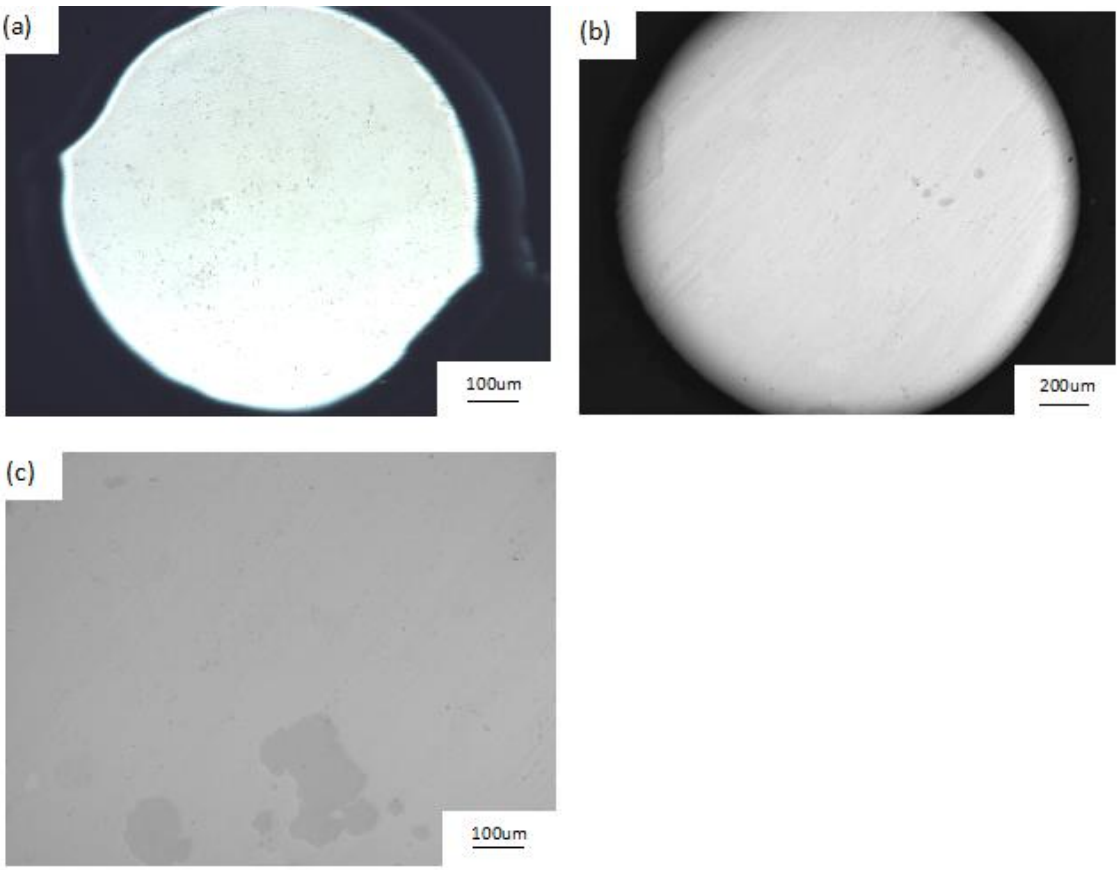

Figure 3. Optical microscopy (OM) images of the cross-sectional microstructures of the $Cu_{45}Zr_{48}Al_4Nb_3$ BMGC samples with different diameters, (**a**) 1, (**b**) 2, (**c**) 3 mm.

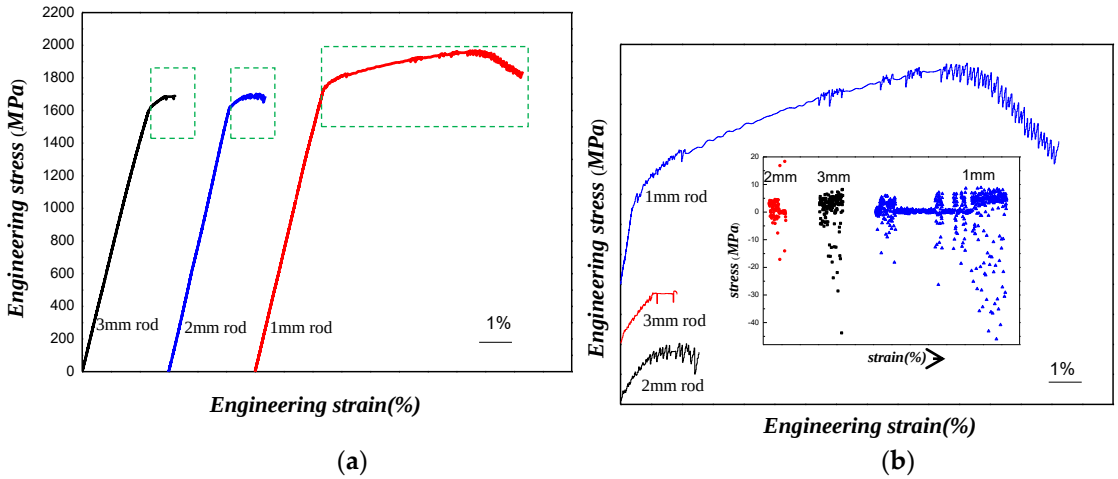

Figure 4. Compression stress–stain curves of the $Cu_{45}Zr_{48}Al_4Nb_3$ BMGC samples with different diameters (**a**), (**b**) is the magnified view of (**a**), and the value of the stress-drop is shown in the inset of Figure (**b**).

The side views and surface morphologies of the compressive fractured $Cu_{45}Zr_{48}Al_4Nb_3$ BMGC samples with different diameters are shown in Figure 5. It can be observed from the figure that shear

fracture was the dominant fracture mode of the samples. Figure 5a–c show that the shear angle of the samples decreased from 49 to 45° with an increase in the sample diameter from 1 to 3 mm. Multiple shear bands were observed on the lateral surface of the 1 mm sample (insets of Figure 5a). The 2 mm and 3 mm samples showed few shear bands (insets of Figure 5b,c). Vein-like structures were visible on the fracture surfaces and some melting regions were formed, as shown in Figure 5a–c. In addition, the sizes and shapes of the vein-like structures observed on the 1 mm sample were completely different from those observed on the other two samples. Typical vein-like patterns appeared on the fracture surfaces of the three samples because of the local viscous flow occurring during the shear deformation process. The vein-like structure was caused by shear band obstruction. Unlike the 1 mm sample, the 2 and 3 mm samples showed few vein-like structures and smooth surfaces and hence poor compressive plasticity [27]. The tear edges and drop patterns can be observed on the fracture surfaces of the 2 mm and 3 mm samples. The vein pattern size of the 1, 2, and 3 mm samples was approximately 13, 18, and 23 um, respectively. The previous study reported that the vein pattern density was connected to the changes of the strength and the plasticity of the specimen, where the larger vein pattern density would lead to a higher strength and plasticity of the specimens. The toughness of the 1, 2, and 3 mm samples was estimated to be 70, 50, and 41 MPa $m^{1/2}$, respectively [2,9].

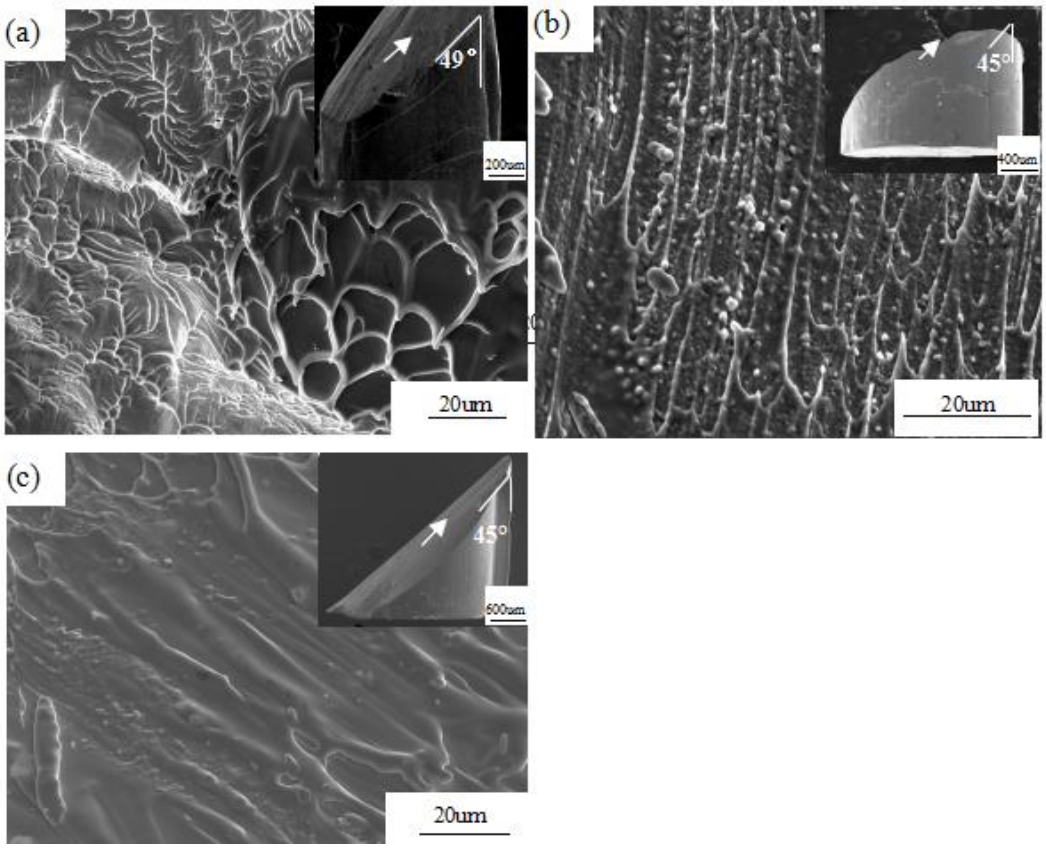

Figure 5. Scanning electron microscopy (SEM) images of the $Cu_{45}Zr_{48}Al_4Nb_3$ bulk metallic glass composite (BMGC) fracture samples with the diameters of 1 mm (**a**), 2 mm (**b**), 3 mm (**c**).

The TEM images of the 3 mm sample are shown in Figure 6. The sample showed some nano-sized crystalline phases on the glassy matrix. These nanocrystalline phases efficiently prevent the discontinuous propagation and branching of the primary shear bands during the compression deformation process. Ning et al. [2] investigated the nanocrystal embedded in the $Cu_{44.3}Zr_{48}Al_4Nb_{3.7}$ alloys, which was confirmed to the B2–CuZr crystals. This implies that the propagation of the shear band may be hindered by the martensite particles in the glassy matrix, as the B2 phase has a positive

impact to prevent the propagation of the shear band. In contrast, the micro-sized crystalline phases present in the 3 mm sample were inefficient for prohibiting the propagation of the shear bands. Kim et al. [28] demonstrated that the crystalline phase fraction of BMGCs is closely related to their yield strength. The yield strength (σ) of the composites was calculated using Equation (1):

$$\sigma_{composite} = f_{amorphous}\sigma_{amorphous} + f_{crystalline}\sigma_{crystalline} \quad (1)$$

where f is the crystalline fraction of the samples. The strength of the amorphous matrix was significantly higher than that of the crystalline phases [29]. The micro-sized crystalline phase content of the 3 mm sample was larger than those of the 1 and 2 mm samples. Hence, the 3 mm sample showed lower yield strength than the other two samples. Another reason for the low yield strength of the 3 mm sample was its strain incompatibility, which appeared between the glassy matrix and the crystalline phase during the plastic flow process and weakened the interface of the sample, leading to its failure [30]. The free volume of an alloy facilitates the migration of atoms in it upon deformation by force [20]. In addition, the free volume acts as the nucleation site for shear bands [31]. Hence, a higher free volume results in easier nucleation and the multiple distribution of shear bands [32]. Thus, it can be stated that the free volume content of the 1 mm sample affected its shear band propagation significantly, as shown in Figure 5a. The presence of a larger number of shear bands in the 1 mm sample (due to its large free volume) improved its compressive plasticity. Hence, the 1 mm BMGCs sample showed larger plasticity than the 3 mm sample.

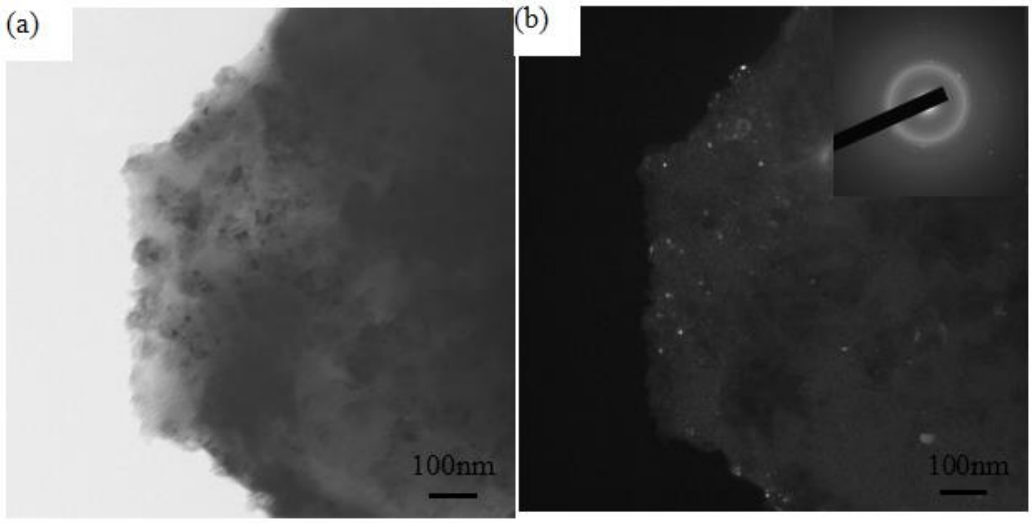

Figure 6. Transmission electron microscopy (TEM) images of the $Cu_{45}Zr_{48}Al_4Nb_3$ BMGC sample with the diameter of 3 mm (**a**,**b**), the inset plot is an diffraction pattern of (**b**).

It is also known that compression tests may be affected by various factors, and the size of the sample may impact the result. Xie et al. [33] believed that when the specimen was tested for compressive mechanical properties, both the system and the specimen would deform elastically. For large-sized specimens, the load on the specimen before breaking was much greater than that on the small-sized specimen, and the amount of elastic deformation of the system and the specimen was also much greater than that of the small-sized specimen. Hence, when a small amount of plastic deformation occurred on the large-sized specimens, the elastic deformation of the system and the specimen would recover, causing additional displacement and strain on the specimen and lead to the rapid instability of the shear band, where the specimen would be severely softened and suddenly broken, showing poor plasticity. Consequently, the plasticity increased with decreasing specimen size in the amorphous alloy, where the results could be attributed to the amount of free volume and the effect of geometric size.

4. Conclusions

The compressive plasticity and yield strength of the 1 mm $Cu_{45}Zr_{48}Al_4Nb_3$ BMGC sample were higher than those of the 2 and 3 mm samples at room temperature. The larger yield strength of the 1 mm sample can be attributed to the presence of a few microsized crystalline phases during the rapid solidification process. This sample exhibited a large free volume and hence higher compressive plasticity. The compression deformation behaviors of the $Cu_{45}Zr_{48}Al_4Nb_3$ BMGC samples were size-dependent.

Author Contributions: Conceptualization, W.L. and Y.C.; methodology, Y.C. and L.W.; validation, Y.W. and K.Q.; writing—original draft preparation, Y.C.; writing—review and editing, W.L.; supervision, X.S. and N.F.; project administration, X.S. and N.F.; funding acquisition, Y.C. All authors have read and agreed to the published version of the manuscript.

Funding: This research was funded by the Fundamental Research Funds for Province Universities under Grant Hkdcx2018010.

Acknowledgments: The authors gratefully acknowledge the financial support of the Fundamental Research Funds for Province Universities (Grant No. Hkdcx2018010).

Conflicts of Interest: The authors declare no conflict of interest.

References

1. Révész, Á.; Kovács, Z. Severe plastic deformation of amorphous alloys(Review). *Mater. Trans.* **2019**, *60*, 1283–1293. [CrossRef]
2. Ning, Z.; Liang, W.; Zhang, M.-X.; Li, Z.; Sun, H.; Liu, A.; Sun, J. High tensile plasticity and strength of a CuZr-based bulk metallic glass composite. *Mater. Des.* **2016**, *90*, 145–150. [CrossRef]
3. Mandal, S.; Kailath, A.J. Enhanced Plasticity of Cu-Zr-Ti Bulk Metallic Glass and Its Correlation with Fragility. *Metall. Mater. Trans. A* **2018**, *50*, 199–208. [CrossRef]
4. Zhou, W.; Hu, J.; Weng, W.; Gao, L.; Xu, G. Enhancement of plasticity in Zr-Cu-Ni-Al-Ti bulk metallic glass by heterogeneous microstructure. *J. Non-Crystalline Solids* **2018**, *481*, 530–536. [CrossRef]
5. Qiao, J.; Chen, Y.H.; Lyu, G.J.; Song, K.K.; Pelletier, J.; Yao, Y. Mechanical Relaxation of a $Ti_{36.2}Zr_{30.3}Cu_{8.3}Fe_4Be_{21.2}$ Bulk Metallic Glass: Experiments and Theoretical Analysis. *Acta Metall. Sin. (Eng. Lett.)* **2018**, *32*, 726–732. [CrossRef]
6. Wang, D.; Chen, Y.; Mu, J.; Zhu, Z.; Zhang, H.; Wang, Y.-D.; An, K. An in situ neutron diffraction study of plastic deformation in a $Cu_{46.5}Zr_{46.5}Al_7$ bulk metallic glass composite. *Scr. Mater.* **2018**, *153*, 118–121. [CrossRef]
7. Szuecs, F.; Kim, C.; Johnson, W. Mechanical properties of $Zr_{56.2}Ti_{13.8}Nb_{5.0}Cu_{6.9}Ni_{5.6}Be_{12.5}$ ductile phase reinforced bulk metallic glass composite. *Acta Mater.* **2001**, *49*, 1507–1513. [CrossRef]
8. Chen, D.; Dong, J.-F.; Ma, G.-Z. Synthesis and compressive fracture behavior of a CuZr-based bulk amorphous alloy with Ti addition. *J. Central South Univ.* **2013**, *20*, 1137–1141. [CrossRef]
9. Li, J.; Jang, J.; Li, C.; Jian, S.; Tsai, P.; Hwang, J.; Huang, J.; Nieh, T. Significant plasticity enhancement of ZrCu-based bulk metallic glass composite dispersed by in situ and ex situ Ta particles. *Mater. Sci. Eng. A* **2012**, *551*, 249–254. [CrossRef]
10. Sun, H.C.; Ning, Z.; Wang, G.; Liang, W.Z.; Pauly, S.; Huang, Y.J.; Guo, S.; Xue, X.; Sun, J.F. In-situ tensile testing of ZrCu-based metallic glass composites. *Sci. Rep.* **2018**, *8*, 4651. [CrossRef]
11. Zhai, H.-M.; Wang, H.-F.; Liu, F. Effect of minor Nb addition on mechanical properties of in-situ Cu-based bulk metallic glass composite. *Trans. Nonferrous Met. Soc. China* **2017**, *27*, 363–368. [CrossRef]
12. Mahmoodan, M.; Gholamipour, R.Z.; Mirdamadi, S.; Nategh, S. Effect of Nb Content on Mechanical Behavior and Structural Properties of $W/(Zr_{55}Cu_{30}Al_{10}Ni_5)_{100-x}Nb_x$ Composite. *Metall. Mater. Trans. A* **2017**, *48*, 2496. [CrossRef]
13. Wang, H.-S.; Wu, J.-Y.; Liu, Y.-T. Effect of the volume fraction of the ex-situ reinforced Ta additions on the microstructure and properties of laser-welded Zr-based bulk metallic glass composites. *Intermetallics* **2016**, *68*, 87–94. [CrossRef]
14. Hofmann, U.C.; Suh, J.-Y.; Wiest, A.; Lind, M.-L.; Demetriou, M.D.; Johnson, W.L. Development of tough, low-density titanium-based bulk metallic glass matrix composites with tensile ductility. *Proc. Natl. Acad. Sci. USA* **2008**, *105*, 20136–20140. [CrossRef]

15. Wang, X.; Jiang, F.; Hahn, H.; Li, J.; Gleiter, H.; Sun, J.; Fang, J. Sample size effects on strength and deformation mechanism of $Sc_{75}Fe_{25}$ nanoglass and metallic glass. *Scr. Mater.* **2016**, *116*, 95–99. [CrossRef]
16. Zhang, Y.; Liu, J.; Chen, S.Y.; Xie, X.; Liaw, P.K.; Dahmen, K.A.; Qiao, J.W.; Wang, Y.L.; Zhang, Y. Serration and noise behaviors in materials. *Prog. Mater. Sci.* **2017**, *90*, 358–460. [CrossRef]
17. Fan, J.; Wu, F.; Li, N. Dynamic compressive response of a dendrite-reinforced Ti-based bulk metallic glass composite. *Mater. Sci. Eng. A* **2018**, *720*, 140–144. [CrossRef]
18. Wu, F.; Zheng, W.; Wu, S.; Zhang, Z.; Shen, J. Shear stability of metallic glasses. *Int. J. Plast.* **2011**, *27*, 560–575. [CrossRef]
19. Xiao, Y.; Wu, Y.; Liu, Z.; Wu, H.-H.; Lü, Z. Effects of cooling rates on the mechanical properties of a Ti-based bulk metallic glass. *Sci. China Ser. G Phys. Mech. Astron.* **2010**, *53*, 394–398. [CrossRef]
20. Liang, M.; Zhu, Y.; Ji, Z.; Fu, J.; Zheng, C. Effect of laser shock peening and its size-dependence on the compressive plasticity of Zr-based bulk metallic glass. *J. Mater. Process. Technol.* **2018**, *251*, 47–53. [CrossRef]
21. Lin, X.H.; Johnson, W.L. Formation of Ti–Zr–Cu–Ni bulk metallic glasses. *J. Appl. Phys.* **1995**, *78*, 6514–6519. [CrossRef]
22. Slipenyuk, A.; Eckert, J. Correlation between enthalpy change and free volume reduction during structural relaxation of $Zr_{55}Cu_{30}Al_{10}Ni_5$ metallic glass. *Scr. Mater.* **2004**, *50*, 39–44. [CrossRef]
23. Okulov, I.; Soldatov, I.; Gokuldoss, P.K.; Sarac, B.; Spieckermann, F.; Eckert, J. Fabrication of Metastable Crystalline Nanocomposites by Flash Annealing of $Cu_{47.5}Zr_{47.5}Al_5$ Metallic Glass Using Joule Heating. *Nanomaterials* **2020**, *10*, 84. [CrossRef] [PubMed]
24. Kaban, I.; Khalouk, K.; Gasser, F.; Gasser, J.-G.; Bednarcik, J.; Shuleshova, O.; Okulov, I.; Gemming, T.; Mattern, N.; Eckert, J. In situ studies of temperature-dependent behaviour and crystallisation of $Ni_{36.5}Pd_{36.5}P_{27}$ metallic glass. *J. Alloys Compd.* **2014**, *615*, S208–S212. [CrossRef]
25. Wu, Y.; Li, H.; Liu, Z.; Chen, G.; Lu, Z. Interpreting size effects of bulk metallic glasses based on a size-independent critical energy density. *Intermetallics* **2010**, *18*, 157–160. [CrossRef]
26. Zhang, Y.; Qiao, J.-W.; Liaw, P.K. A Brief Review of High Entropy Alloys and Serration Behavior and Flow Units. *J. Iron Steel Res. Int.* **2016**, *23*, 2–6. [CrossRef]
27. He, M.; Zhang, Y.; Xia, L.; Yu, P. Kinetics and thermal stability of the $Ni_{62}Nb_{38-x}Ta_x$ (x=5, 10, 15, 20 and 25) bulk metallic glasses. *Sci. China Ser. G Phys. Mech. Astron.* **2017**, *60*, 42. [CrossRef]
28. Kim, B.J.; Yun, Y.S.; Kim, W.T.; Kim, D. Phase formation and mechanical properties of Cu-Zr-Ti bulk metallic glass composites. *Met. Mater. Int.* **2016**, *22*, 1026–1032. [CrossRef]
29. Narayan, R.L.; Singh, P.; Hofmann, D.; Hutchinson, N.; Flores, K.; Ramamurty, U. On the microstructure–tensile property correlations in bulk metallic glass matrix composites with crystalline dendrites. *Acta Mater.* **2012**, *60*, 5089–5100. [CrossRef]
30. Chung, T.-M.; Jian, S.-R.; Hsieh, P.-J. The Effect of Ag Addition on the Enhancement of the Thermal and Mechanical Properties of CuZrAl Bulk Metallic Glasses. *Metals* **2016**, *6*, 216. [CrossRef]
31. Chen, L.; Fu, Z.D.; Zhang, G.Q.; Hao, X.P.; Jiang, Q.K.; Wang, X.D.; Cao, Q.P.; Franz, H.; Liu, Y.G.; Xie, H.S.; et al. New Class of Plastic Bulk Metallic Glass. *Phys. Rev. Lett.* **2008**, *100*, 075501. [CrossRef] [PubMed]
32. Sun, H.; Ning, Z.; Ren, J.; Liang, W.; Huang, Y.; Sun, J.; Xue, X.; Wang, G. Serration and shear avalanches in a ZrCu based bulk metallic glass composite in different loading methods. *J. Mater. Sci. Technol.* **2019**, *35*, 2079–2085. [CrossRef]
33. Xie, S.; George, E.P. Size-dependent plasticity and fracture of a metallic glass in compression. *Intermetallics* **2008**, *16*, 485–489. [CrossRef]

© 2020 by the authors. Licensee MDPI, Basel, Switzerland. This article is an open access article distributed under the terms and conditions of the Creative Commons Attribution (CC BY) license (http://creativecommons.org/licenses/by/4.0/).